Theoretical spectral function of CH3NH3PbI3 hybrid perovskite around the Fermi level

Min-I Lee, S. Ayaz Khan, J. Minar, Antonio Tejeda

Theoretical spectral function of $CH_3NH_3PbI_3$ hybrid perovskite around the Fermi level

Min-I Lee,[1] S. Ayaz Khan,[2] J. Minar,[2] and A. Tejeda[1,*]

[1] *Laboratoire de Physique des Solides, CNRS, Univ. Paris-Sud, Université Paris-Saclay, 91405 Orsay, France*
[2] *New Technologies - Research Center, University of West Bohemia, Univerzitni 8, 306 14 Pilsen, Czech Republic*

Methylammonium lead iodide $CH_3NH_3PbI_3$ (MAPI) is one of the hybrid organic-inorganic perovskites (HOIPs) widely considered for photovoltaic devices. Since photoemission is possibly the best technique for the experimental determination of the bands, we have calculated photoemission spectra at the main photon energies available at conventional laboratories (He I - 21.2 eV, He II - 40.8 eV) by performing fully relativistic Spin-Polarized Relativistic Korringa-Kohn-Rostoker (SPRKKR) calculations. Similarly, we have studied how s- and p-polarization affect to the calculated spectra. These studies could help to reach a better understanding of photoemission measurements on MAPI.

I. INTRODUCTION

Hybrid organic-inorganic perovskites (HOIPs) have attracted considerable interest in the field of photovoltaics owing to their strong light absorption along with the low cost solution-based fabrication process[1–4]. The power conversion efficiency (PCE) of the perovskite cells has dramatically reached an efficiency exceeding the latest record of 25.7% in 2022[5]. Among all kinds of HOIPs, the three-dimensional perovskite methylammonium lead iodide ($CH_3NH_3PbI_3$, $MAPbI_3$, or MAPI) is one of the most commonly used materials in perovskite cells.

To improve the efficiency of any photovoltaic material, it is important to have a good understanding of its electronic properties, such as the band gap, the electronic localization and the charge carrier mobility in the material. Most of this information can be obtained from the electronic band structure. Photoemission spectroscopy is the best technique for experimentally measuring the valence band with surface sensitivity[6–11]. In hybrid perovskites, important variations in the electronic structure have been reported[12–14], which can impact the understanding of the interfacial physics between hybrid perovskites and charge transport layers in solar cells.

Comparing experimental and calculated bands can be very helpful when controversies related to the electronic structure subsist. Measuring MAPI in the most widespread photoemission setups rely on the use of discharge lamps as photon sources (with $h\nu = 21.2$ or 40.8 eV, i.e., He I and He II lines, respectively). However, comparing experimental measurements of MAPI with calculations is not straightforward. The reason is that MAPI is a three dimensional material and therefore measurements using discharge lamps explore correspond to a k perpendicular to the surface that is not in a high-symmetry plane of the reciprocal space.

In order to properly analyze the experimental data, theoretical calculations including the photoemission process are needed. The reason is that the transition probabilities of the optical excitation by photons depend on the experimental geometry (angle between exciting photons and emitted electrons, explored Brillouin zone, light polarization, photon energy...). Therefore the spectral weight of some electronic states can significantly vary, that is technically known as matrix element effects. These unavoidable effects can considerably affect photoemission spectra since, in the most critical cases, the initial state intensity could even be suppressed[15]. The influence of matrix element effects has been observed in our previous experimental angle-resolved photoemission spectroscopy measurements for MAPI[16].

To compare with experimental results, theoretical band structure studies are essential. Density func-

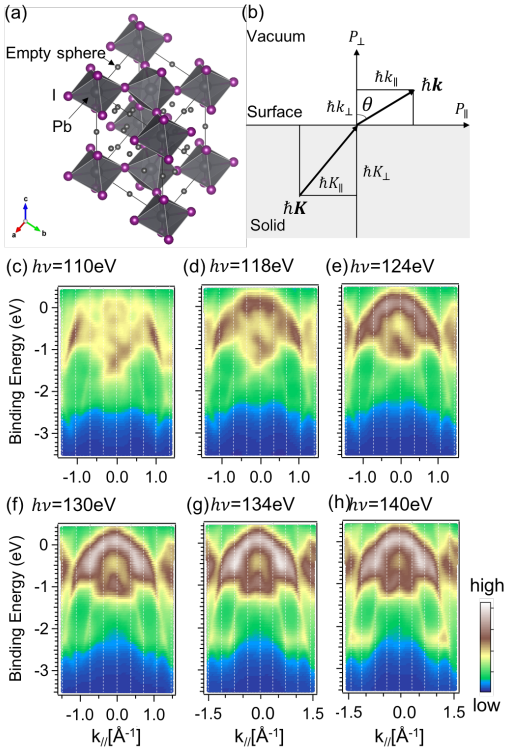

FIG. 1. (a) Atomic structure of MAPI including the empty shperes considered in the calculations. (b) Photoelectrons conserve their parallel wavevector when crossing the solid/vacuum interface but the perpendicular wavevector decreases when crossing the interface. Calculated angle-resolved photoemission spectroscopy (ARPES) valence band spectrum of MAPI for different photon energies: (c) 110 eV, (d) 118 eV, (e) 124 eV, (f) 130 eV, (g) 134 eV, (h) 140 eV.

tional theory (DFT)[17–25], GW[23,24,26] and tight binding calculations[27] have been extensively used to determine the ground state band structure and the density-of-states (DOS). However these calculations do not take into account the matrix element effects of the photoemission process. In this work, we present the theoretical calculation of the k-resolved photoemission spectra of MAPI at the most common situations in conventional laboratories, simulating experimental spectra along non-high symmetry directions and taking into account matrix element effects. This is a valuable information for comparison of experimental and theoretical electronic properties of MAPI and derived compounds.

Angle-resolved photoemission spectroscopy (ARPES) is a very extended technique to experimentally determine the electronic structure of solids. In three dimensional systems as $CH_3NH_3PbI_3$, it is necessary to use particular photon energies to measure the electronic structure along high symmetry directions, because there is dispersion along $k_\perp$ that depends on the photon energy, as it can be observed for MAPI in Fig. 1. It should be mentioned that the problem of measuring a three-dimensional system in photoemission is shown in Fig. 1(b), where the parallel wavevector of the photoelectron is conserved at the vacuum/solid interface, but not the perpendicular wavevector. Unless the measurement is performed at a synchrotron facility, arbitrary photon energies are not available. In most of conventional laboratories dealing with these photovoltaic materials, the photon energies usually correspond to He I or II lines, which correspond to an arbitrary $k_\perp$ of MAPI. Since the theoretical bands are usually calculated along the high-symmetry directions, it is extremely useful to know the expected band structure that is actually measured with a He lamp. Moreover, standard calculations focus only on the band structure and do not describe the photoemission process, where the photoemission probability can significantly affect the intensity of a given electronic state, rendering sometimes difficult the theory-experiment comparison. In this article, we study the electronic structure of MAPI using common photon energies at conventional laboratories by taking into account the matrix element effects, which had not been previously addressed in the literature.

II. METHODS

Self-consistent electronic structure calculations were performed within the ab-initio framework of spin–density functional theory. The electronic structure was calculated in a fully relativistic mode by solving the corresponding Dirac equation. This was achieved using the relativistic multiple-scattering or Spin-Polarized Relativistic Korringa-Kohn-Rostoker (SPRKKR) formalism[28–30]. The Vosko, Wilk and Nusair local density approximation (VWN-LDA)[31] was used to approximate the exchange correlation part of the potential. The resulting electronic structure represented

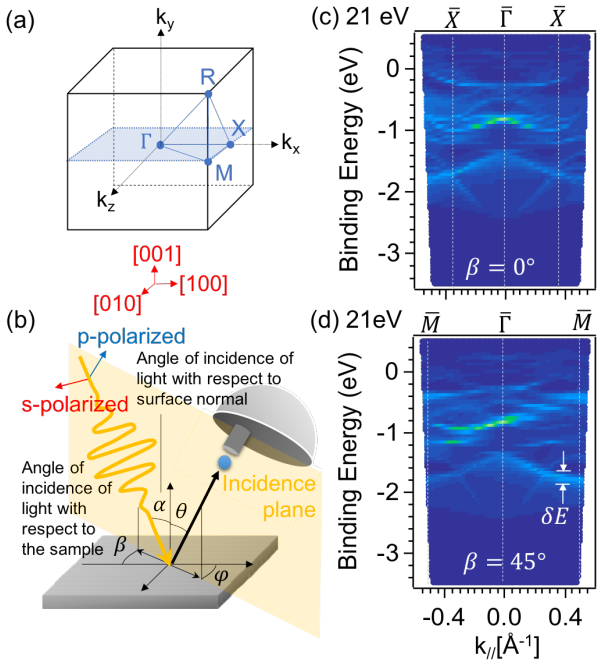

FIG. 2. (a) Brillouin zone for a cubic phase of MAPI. (b) Sketch of the geometry used in calculations. The incidence-light plane is perpendicular to the sample surface, defined by the azimuthal angle β of light incidence. The electric vector of the incident light is parallel and perpendicular to the incident light plane for the p- and s-polarization, respectively. Simulated ARPES spectra for a photon energy of He I (21 eV) along directions (c) $\overline{X\Gamma X}$ parallel to $X\Gamma X$ and (d) $\overline{M\Gamma M}$ parallel to $M\Gamma M$.

by single-site scattering for the different atoms and the corresponding quantities related to initial and final-state were used as input for photocurrent calculations. Our spectroscopic analysis is based on the fully relativistic one-step model in its spin–density matrix formulation[32], originally proposed by Pendry *et al.*[33]. This allows to include all the matrix-element effects induced by the experimental geometry: i.e. incoming photon and outgoing photoelectron angles, light polarization and final-state effects. The influence of impurity scattering, defects and thermal vibrations on the lifetime are taken into account through a small constant imaginary potential term Im for the initial state, added to the single particle potential. The final state is constructed within the formalism for spin-polarized low-energy electron diffraction (SPLEED) by a spin-polarized time-reversed LEED state[33]. The finite imaginary part of the effective potential of the final state simulates the inelastic mean free path.

Considering the whole unit cell of MAPI is beyond current possibilities of SPRKKR calculations, due to the large number of atoms. An approximation is therefore necessary to describe the photoemission process by taking into account the states dispersing and contributing more at the top of the valence band. Molecular states do not contribute significantly at the top of the valence

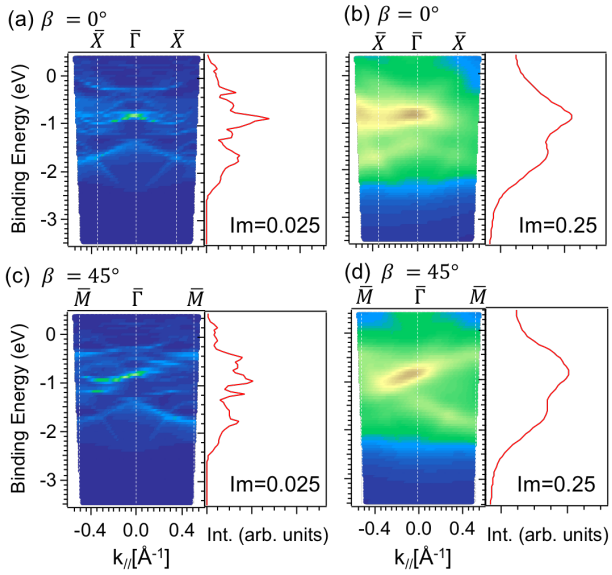

FIG. 3. ARPES spectrum at 21 eV using p-polarized photons (polarization perpendicular to the sample surface) along directions parallel to (a) $\overline{XΓX}$ and (c) $\overline{MΓM}$, with $Im = 0.025$ Ryd and spectral bandwidths δE around 100 meV ± 50 meV. (b) $\overline{XΓX}$ and (d) $\overline{MΓM}$, with $Im = 0.25$ Ryd, the spectral bandwidths δE is about 4 times wider (400 meV ± 100 meV). The red curves on the right of each panel are computed angle-integrated spectra.

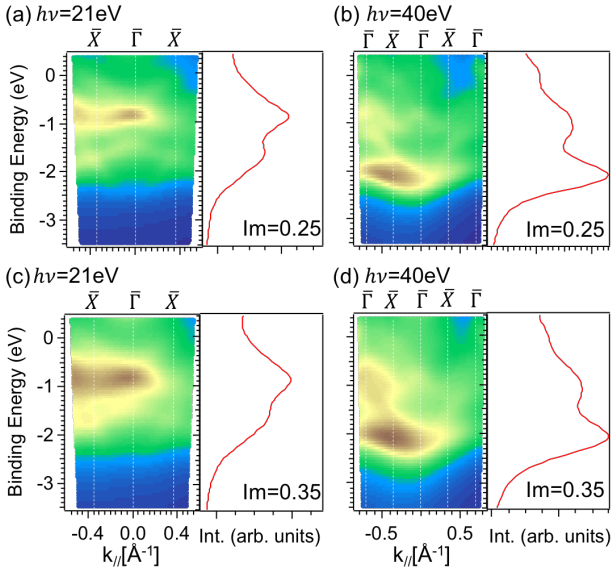

FIG. 4. ARPES spectrum along $\overline{XΓX}$ and its corresponding angle-integrated spectrum for photon energies (a) (c) 21 eV and (b) (d) 40 eV, to compare with $h\nu = 21.2$ eV (He I) or 40.8 eV (He II). The comparison of different initial state imaginary coefficients, Im=0.25 Ryd and 0.35 Ryd for (a) (b), and (c) (d), respectively. The red curves on the right of each panel are computed angle-integrated spectra.

band (0 eV ~ -4 eV)[34] and they are almost dispersionless. Since the more dispersing features arise from the inorganic part[35], calculations can be performed just with the inorganic part PbI_3 and an appropriate charge transfer, without taking account the details of methylammonium ($CH_3NH_3PbI_3$). The molecular potential is reproduced by using empty spheres, as shown in Fig. 1(a). The use of these empty spheres is a standard procedure to fill interstitial positions with additional scattering centers[35]. In our case twenty four empty spheres were included in the unit cell. Furthermore, we used a 14×14×14 integration mesh. The light polarization was p-polarized at incidence angles of $\alpha = -45°$ with respect to surface normal, and $\beta = 0°$ and 45° with respect to the sample, as shown in Fig. 2(b).

III. RESULTS AND DISCUSSION

Fig. 2(a) shows a cubic Brillouin zone of MAPI and indicates the high symmetry points and the high symmetry directions (continuous lines). In order to measure the electronic bands along the high symmetry direction $ΓMX$ it is necessary to select the correct crystal direction of the sample, which is the ky axis, perpendicular to the sample surface first and rotate the sample around the ky to measure $k_{||}$ spectra along X ($\beta = 0°$) and M ($\beta = 45°$). At the same time, the incident angle of the light with respect to surface normal (α = -45°) is kept unchanged.. Panel (b) presents a sketch of the geometry used for calculations. A He lamp does not allow to measure the $ΓMX$ plane but the projection of it $\overline{ΓMX}$. The photoemission spectra when measuring at $h\nu = 21$ eV (He I line) with the sample normal being the [010] direction are shown in panels (c) and (d) respectively. Due to the matrix element effects, spectral intensities are very different at both sides of $\overline{Γ}$ (panels (c) and (d)). This is also seen along $\overline{MΓM}$ (panel (d)).

In the calculations, the spectral features width δE in Fig. 2 is much narrower than that of experimental bands[36,37]. The spectral width is related to the finite lifetime of the conduction band excitations as well as to the excitation of other degrees of freedom when the photoelectron is kicked off the solid[16]. In SPRKKR, spectral widths can be adjusted by tuning the imaginary part of the initial state potential Im, while setting the imaginary part in the effective potential for the final state at 3 eV[32]. Fig. 3 (a) and (c) shows simulations of the valence band along $\overline{XΓX}$ and $\overline{MΓM}$ for a spectral bandwidth of 100 meV ± 50 meV corresponding to $Im = 0.025$ Ryd, which allow a clear identification of the bands. In order to reproduce experiments[37], we show in Fig. 3 (b) and (d), calculations with $Im = 0.25$ Ryd, with a spectral width δE about 4 times wider (400 meV ± 100 meV). Now only two broad features are seen in panel (b), that correspond to the band around -1 eV and the band dispersing from -1.8 eV to -1.4 eV. Panel (d) shows similarly two broad features, dispersing from -1 eV to -0.5 eV and from -1 eV to -2 eV. The effect of considering different Im is also

evident in the angle-integrated spectra, as more peaks appear for $Im = 0.025$ Ryd. More details of broadening effects had been discussed in the reference[38].

In conventional laboratories, He II line (40 eV) is also commonly accessible, and it allows to explore larger regions of the reciprocal space. Fig. 4 compares the simulated spectra at He I (21 eV) and He II (40 eV) along directions with an identical $k_{||}$ projection although a different $k_{\perp}$ (see fig. 2). The imaginary part of the initial state potential Im has been set to 0.25 Ryd for (a), (b) and to 0.35 Ryd for (c), (d). Fig. 4 shows that at 21 eV the maximum spectral weight appears for binding energies around -0.8 eV (see the integrated spectra). On the other hand, for hν= 40 eV the maximal intensity appears at the bottom of the valence band (around -2 eV) while the band around -0.8 eV is very faint. Similarly, the most intense band at 40 eV almost disappears for 21 eV.

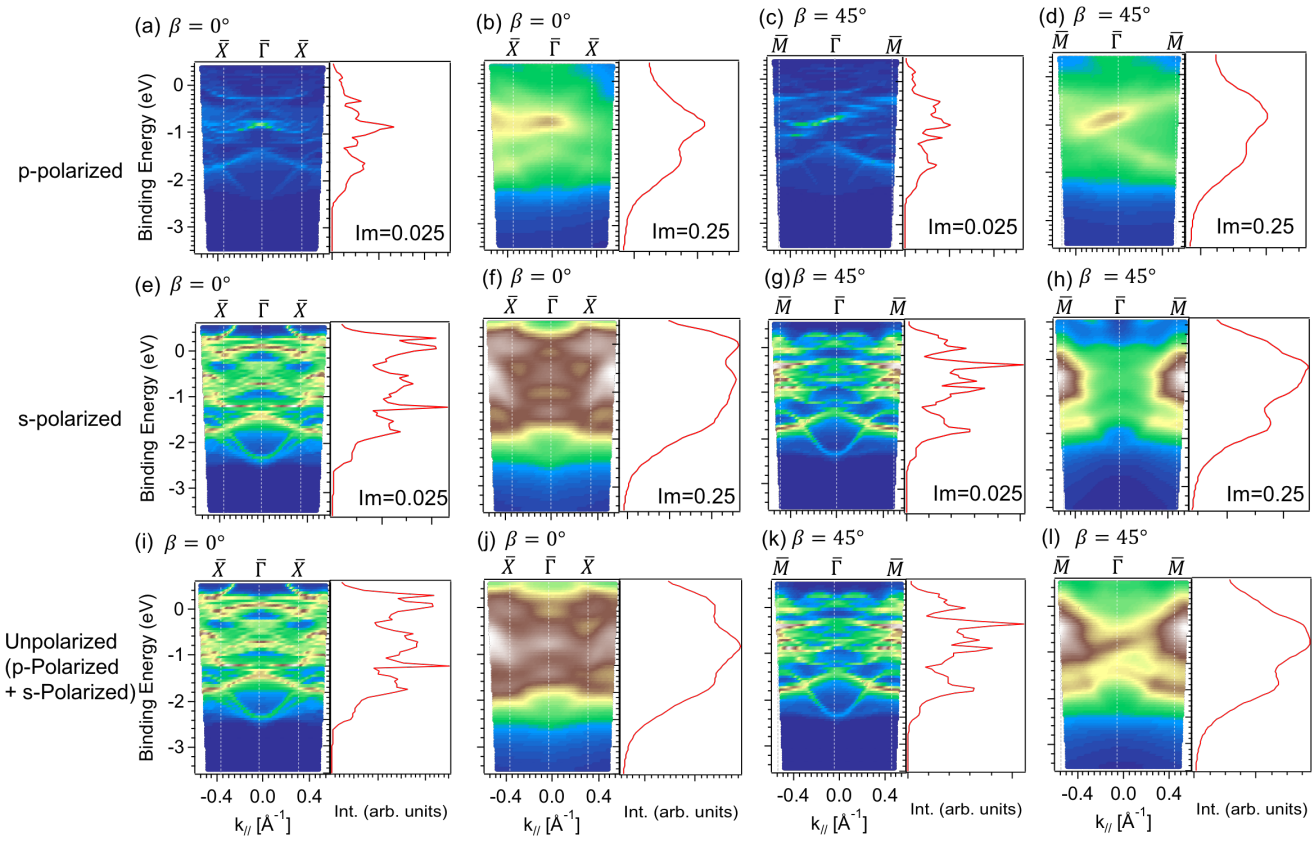

FIG. 5. ARPES spectra for different light polarizations and unpolarized light at a photon energy of 21 eV for $\overline{X\Gamma X}$ and for $\overline{M\Gamma M}$. $Im = 0.025$ Ryd and $Im = 0.25$ Ryd have been considered. The red curves on the right of each panel are computed angle-integrated spectra.

Depending on the light polarization, spectra can vary significantly in general, as we will see that it is the case for MAPI. Indeed the photoemission intensity is:[39]

$$I(\mathbf{k}_{\parallel}, \omega) = I_0(\mathbf{k}_{\parallel}, \nu, \mathbf{A}) f(\omega) A(\mathbf{k}_{\parallel}, \omega), \qquad (1)$$

where ω is the electron energy with respect to the Fermi level. $I_0(\mathbf{k}_{\parallel}, \nu, \mathbf{A})$), according to Fermi's golden rule, is proportional to the squared one-electron matrix element $\left|M_{f,i}^{\mathbf{k}_{\parallel}}\right|^2 \propto \left|\left\langle \phi_f^{\mathbf{k}_{\parallel}} \left| \boldsymbol{\varepsilon} \cdot \mathbf{x} \right| \phi_i^{\mathbf{k}_{\parallel}} \right\rangle\right|$, where $\boldsymbol{\varepsilon}$ is a unit vector along the polarization direction of the vector potential $\mathbf{A}$. Therefore, the intensity depends on the electron momentum, on the energy and the polarization of the incoming photon. Well-defined polarizations are p-polarization and s-polarization, where the electrical field is respectively perpendicular or parallel to the sample surface. Fig. 5 shows the simulations for these two polarizations and for the unpolarized light at $h\nu = 21$ eV. The simulation for unpolarized light was determined by adding p- and s-polarization calculations, after normalizing their maximum value to 1, since the code does not provide comparable intensities for different polarizations. A strong influence of the polarization is observed. Comparing different light polarizations, it is observed that the intensity of the bands is much more stronger in s-polarization both along $\overline{X\Gamma X}$ and $\overline{M\Gamma M}$. The intensity of the dispersions suppressed for p-polarization especially at $\overline{X}$ and $\overline{M}$. In addition, the asymmetric distributions can be observed in Fig. 5(a,b,c,d) and the symmetric ones can be observed in Fig. 5 (e,f,g,h). The symmetry of the dispersions depends thus on the polarization of the light: the observed distributions are asymmetric

for p-polarization and symmetric for s-polarization.

IV. CONCLUSIONS

In conclusion, we present calculations for the ARPES spectra for methylammonium lead iodide for the most common photon energies used in conventional laboratories. The formalism for calculations is the fully relativistic Spin-Polarized Relativistic Korringa-Kohn-Rostoker (SPRKKR) that takes into account the photoemission process, allowing thus a straightforward comparison to experimental data. The comparison to experimental data in a three dimensional system as MAPI is also simplified by calculations of ARPES spectra at the He lamp energies. We have also studied the influence of matrix elements at different Brillouin zones and light polarizations. We believe that these calculations will be a reference for future measurements on this system.

ACKNOWLEDGMENTS

The project leading to this article has received funding from the European Union's Horizon 2020 research and innovation program under grant agreement No 687008 (GOTSolar). We also acknowledge the support from University of West Bohemia, New Technologies - Research Center's group members for the calculations and the funding for the cooperation from Computational and Experimental Design of Advanced Materials with New Functionalities (CEDAMNF; grant CZ.02.1.01/0.0/0.0/15_003/0000358) of the Ministry of Education, Youth and Sports (Czech Republic). We also thank A. Zobelli for helpful discussions.

* antonio.tejeda@cnrs.fr

[1] Zengxi Wei, Yuhang Zhao, Jie Jiang, Weibo Yan, Yuezhan Feng, and Jianmin Ma. Research progress on hybrid organic–inorganic perovskites for photo-applications. *Chinese Chemical Letters*, 31(12):3055–3064, 2020.

[2] Martin A Green, Anita Ho-Baillie, and Henry J Snaith. The emergence of perovskite solar cells. *Nature photonics*, 8(7):506–514, 2014.

[3] Nam Joong Jeon, Jun Hong Noh, Young Chan Kim, Woon Seok Yang, Seungchan Ryu, and Sang Il Seok. Solvent engineering for high-performance inorganic–organic hybrid perovskite solar cells. *Nature materials*, 13(9):897, 2014.

[4] Julian Burschka, Norman Pellet, Soo-Jin Moon, Robin Humphry-Baker, Peng Gao, Mohammad K Nazeeruddin, and Michael Grätzel. Sequential deposition as a route to high-performance perovskite-sensitized solar cells. *Nature*, 499(7458):316, 2013.

[5] Best research-cell efficiency chart, https://www.nrel.gov/pv/cell-efficiency.html, 2021.

[6] YM Lee, I Maeng, MQ Lyu, JH Yun, LZ Wang, M Nakamura, and MC Jung. Bias effect on surface chemical states of ch3nh3pbbr3 hybrid perovskite single crystal: Decreasing ch3nh2 molecular defect. *Applied Surface Science*, 542:148536, 2021.

[7] M Kot, M Vorokhta, ZP Wang, HJ Snaith, D Schmeisser, and JI Flege. Thermal stability of ch3nh3pbixcl3-x versus [hc(nh2)(2)](0.83)cs0.17pbi2.7br0.3 perovskite films by x-ray photoelectron spectroscopy. *Applied Surface Science*, 513:145596, 2020.

[8] A Damascelli. Probing the electronic structure of complex systems by arpes. *Physica Scripta*, T109:61, 2004.

[9] A Schwobel, R Precht, M Motzko, MAC Solano, W Calvet, R Hausbrand, and W Jaegermann. Determination of the valence band structure of an alkali phosphorus oxynitride glass: A synchrotron xps study on lipon. *Applied Surface Science*, 321:55, 2014.

[10] T Komesu, X Huang, TR Paudel, YB Losovyj, X Zhang, EF Schwier, Y Kojima, MT Zheng, H Iwasawa, K Shimada, MI Saidaminov, D Shi, AL Abdelhady, OM Bakr, S Dong, EY Tsymbal, and PA Dowben. Surface electronic structure of hybrid organo lead bromide perovskite single crystals. *Journal of Physical Chemistry C*, 120:21710, 2016.

[11] JJ Paggel, T Miller, DA Luh, and TC Chiang. Quantum well photoemission from atomically uniform ag films: determination of electronic band structure and quasi-particle lifetime in ag(100). *Applied Surface Science*, 162:78, 2000.

[12] F Zu, Amsalem P, M Ralaiarisoa, T Schultz, R Schlesinger, and N Koch. Surface state density determines the energy level alignment at hybrid perovskite/electron acceptors interfaces. *ACS Appl. Mater. Interfaces*, 9:41546, 2017.

[13] C. Wang, C. Wang, X. Liu, J. Kauppi, Y. Shao, Z. Xiao, C. Bi, J. Huang, and Gao Y. Electronic structure evolution of fullerene on ch3nh3pbi3. *Applied Physics Letters*, 106:111603, 2015.

[14] P. Schulz, L. L. Whittaker-Brooks, B. A. MacLeod, D. C. Olson, Y.-L. Loo, and A Kahn. Electronic level alignment in inverted organometal perovskite solar cells. *Adv. Mater. Interfaces*, 2:1400532, 2015.

[15] Simon Moser. An experimentalist's guide to the matrix element in angle resolved photoemission. *Journal of Electron Spectroscopy and Related Phenomena*, 214:29–52, 2017.

[16] Min-I Lee, Ana Barragán, Maya N Nair, Vincent LR Jacques, David Le Bolloc'h, Pierre Fertey, Khaoula Jemli, Ferdinand Lédée, Gaëlle Trippé-Allard, Emmanuelle Deleporte, et al. First determination of the valence band dispersion of ch3nh3pbi3 hybrid organic–inorganic perovskite. *Journal of Physics D: Applied Physics*, 50(26):26LT02, 2017.

[17] Wei Geng, Le Zhang, Yan-Ning Zhang, Woon-Ming Lau, and Li-Min Liu. First-principles study of lead iodide perovskite tetragonal and orthorhombic phases for photovoltaics. *The Journal of Physical Chemistry C*, 118(34):19565–19571, 2014.

[18] T Umebayashi, K Asai, T Kondo, and A Nakao. Electronic structures of lead iodide based low-dimensional crystals. *Physical Review B*, 67(15):155405, 2003.

[19] Tom Baikie, Yanan Fang, Jeannette M Kadro, Martin Schreyer, Fengxia Wei, Subodh G Mhaisalkar, Michael

Graetzel, and Tim J White. Synthesis and crystal chemistry of the hybrid perovskite (ch 3 nh 3) pbi 3 for solid-state sensitised solar cell applications. *Journal of Materials Chemistry A*, 1(18):5628–5641, 2013.

[20] Paolo Umari, Edoardo Mosconi, and Filippo De Angelis. Relativistic gw calculations on ch 3 nh 3 pbi 3 and ch 3 nh 3 sni 3 perovskites for solar cell applications. *Scientific reports*, 4:4467, 2014.

[21] Wan-Jian Yin, Ji-Hui Yang, Joongoo Kang, Yanfa Yan, and Su-Huai Wei. Halide perovskite materials for solar cells: a theoretical review. *Journal of Materials Chemistry A*, 3(17):8926–8942, 2015.

[22] Jacky Even, Laurent Pedesseau, M-A Dupertuis, J-M Jancu, and Claudine Katan. Electronic model for self-assembled hybrid organic/perovskite semiconductors: Reverse band edge electronic states ordering and spin-orbit coupling. *Physical Review B*, 86(20):205301, 2012.

[23] Anna Amat, Edoardo Mosconi, Enrico Ronca, Claudio Quarti, Paolo Umari, Md K Nazeeruddin, Michael Grätzel, and Filippo De Angelis. Cation-induced band-gap tuning in organohalide perovskites: interplay of spin–orbit coupling and octahedra tilting. *Nano letters*, 14(6):3608–3616, 2014.

[24] Weiwei Gao, Xiang Gao, Tesfaye A Abtew, Yi-Yang Sun, Shengbai Zhang, and Peihong Zhang. Quasiparticle band gap of organic-inorganic hybrid perovskites: Crystal structure, spin-orbit coupling, and self-energy effects. *Physical Review B*, 93(8):085202, 2016.

[25] Fan Zheng, Hiroyuki Takenaka, Fenggong Wang, Nathan Z Koocher, and Andrew M Rappe. First-principles calculation of the bulk photovoltaic effect in ch3nh3pbi3 and ch3nh3pbi3–x cl x. *The journal of physical chemistry letters*, 6(1):31–37, 2014.

[26] Federico Brivio, Keith T Butler, Aron Walsh, and Mark Van Schilfgaarde. Relativistic quasiparticle self-consistent electronic structure of hybrid halide perovskite photovoltaic absorbers. *Physical Review B*, 89(15):155204, 2014.

[27] George C Papavassiliou, IB Koutselas, A Terzis, and M-H Whangbo. Structural and electronic properties of the natural quantum-well system (c6h5ch2ch2nh3) 2sni4. *Solid state communications*, 91(9):695–698, 1994.

[28] Hubert Ebert, Diemo Koedderitzsch, and Jan Minar. Calculating condensed matter properties using the kkr-green's function method—recent developments and applications. *Reports on Progress in Physics*, 74(9):096501, 2011.

[29] H Ebert et al. The munich spr-kkr package, version 7.7, h. ebert et al, 2017.

[30] J. Minár, J. Braun, S. Mankovsky, and H. Ebert. Calculation of angle-resolved photo emission spectra within the one-step model of photo emission—recent developments. *Journal of Electron Spectroscopy and Related Phenomena*, 184(3):91–99, 2011. Advances in Vacuum Ultraviolet and X-ray Physics.

[31] Seymour H Vosko, Leslie Wilk, and Marwan Nusair. Accurate spin-dependent electron liquid correlation energies for local spin density calculations: a critical analysis. *Canadian Journal of physics*, 58(8):1200–1211, 1980.

[32] Jürgen Braun, Jan Minar, and Hubert Ebert. Correlation, temperature and disorder: Recent developments in the one-step description of angle-resolved photoemission. *Physics Reports*, 740:1–34, 2018.

[33] JB Pendry. Theory of photoemission. *Surface Science*, 57(2):679–705, 1976.

[34] Alex M Ganose, Christopher N Savory, and David O Scanlon. (ch3nh3) 2pb (scn) 2i2: A more stable structural motif for hybrid halide photovoltaics? *The journal of physical chemistry letters*, 6(22):4594–4598, 2015.

[35] Min-I Lee, Saleem Ayaz Khan, Hela Mrezguia, Ana Barragán, Maya N Nair, Hamza Khelidj, Younal Ksari, Luca Giovanelli, Jean-Marc Themlin, Ferdinand Lédée, et al. Renormalization of the valence and conduction bands of (c6h5c2h4nh3) 2pbi4 hybrid perovskite. *Journal of Physics D: Applied Physics*, 54(36):365301, 2021.

[36] Fengshuo Zu, Patrick Amsalem, David A Egger, Rongbin Wang, Christian M Wolff, Honghua Fang, Maria Antonietta Loi, Dieter Neher, Leeor Kronik, Steffen Duhm, et al. Constructing the electronic structure of ch3nh3pbi3 and ch3nh3pbbr3 perovskite thin films from single-crystal band structure measurements. *The journal of physical chemistry letters*, 10(3):601–609, 2019.

[37] Jin-Peng Yang, Matthias Meissner, Takuma Yamaguchi, Xiu-Yun Zhang, Takahiro Ueba, Li-Wen Cheng, Shinichiro Ideta, Kiyohisa Tanaka, Xiang-Hua Zeng, Nobuo Ueno, et al. Band dispersion and hole effective mass of methylammonium lead iodide perovskite. *Solar RRL*, 2(10):1800132, 2018.

[38] Yasuo Nakayama, Satoshi Kera, and Nobuo Ueno. Photoelectron spectroscopy on single crystals of organic semiconductors: experimental electronic band structure for optoelectronic properties. *Journal of Materials Chemistry C*, 8(27):9090–9132, 2020.

[39] Andrea Damascelli, Zahid Hussain, and Zhi-Xun Shen. Angle-resolved photoemission studies of the cuprate superconductors. *Reviews of modern physics*, 75(2):473, 2003.